Carbohydrate Polymers 102 (2014) 306–316

Contents lists available at ScienceDirect

Carbohydrate Polymers

journal homepage: www.elsevier.com/locate/carbpol

High-water-content mouldable polyvinyl alcohol-borax hydrogels reinforced by well-dispersed cellulose nanoparticles: Dynamic rheological properties and hydrogel formation mechanism

Jingquan Han[a,b], Tingzhou Lei[c], Qinglin Wu[b,*]

[a] College of Material Science and Engineering, Nanjing Forestry University, Nanjing 210037, China
[b] School of Renewable Natural Resources, Louisiana State University AgCenter, Baton Rouge, LA 70803, United States
[c] Henan Key Laboratory of Biomass Energy, 29 Huayuan Road, Zhengzhou 45008, China

ARTICLE INFO

Article history:
Received 2 August 2013
Received in revised form 19 October 2013
Accepted 27 November 2013
Available online 4 December 2013

Keywords:
Hydrogel
Cellulose nanocrystals
Self-recovery
Rheological properties
Polyvinyl alcohol
Thermo-reversibility

ABSTRACT

Cellulose nanoparticle (CNP) reinforced polyvinyl alcohol-borax (PB) hydrogels were produced via a facile approach in an aqueous system. The effects of particle size, aspect ratio, crystal structure, and surface charge of CNPs on the rheological properties of the composite hydrogels were investigated. The rheological measurements confirmed the incorporation of well-dispersed CNPs to PB system significantly enhanced the viscoelasticity and stiffness of hydrogels. The obtained free-standing, high elasticity and mouldable hydrogels exhibited self-recovery under continuous step strain and thermo-reversibility under temperature sweep. With the addition of cellulose I nanofibers, a 19-fold increase in the high-frequency plateau of storage modulus was obtained compared with that of the pure PB. CNPs acted as multifunctional crosslinking agents and nanofillers to physically and chemically bridge the 3D network hydrogel. The plausible mechanism for the multi-complexation between CNPs, polyvinyl alcohol and borax was proposed to understand the relationship between the 3D network and hydrogel properties.

1. Introduction

Hydrogels are soft, viscoelastic and cross-linked (physically and/or chemically) three-dimensional networks of hydrophilic polymer that can hold large amounts of water and/or biological solution, while maintaining their structural integrity during deformation (Yang et al., 2012; Yang, Liu, Chen, Yu, & Zhu, 2008). Due to their excellent hydrophilicity, permeability, ability to mimic human tissues, hydrogels are particularly attractive in biological, pharmaceutical, and daily-care applications, such as real-time immunoassay, contact lenses, vehicles for drug delivery, cell encapsulation, implantable artificial muscles and organs, and biosensors (Sun et al., 2012; Yang, Han, Duan, Xu, & Sun, 2013). The growing environmental awareness recently has triggered interests in more environmentally friendly and biodegradable hydrogels (Zhang et al., 2011). Due to the hydroxyl groups of each repeating molecular unit, hydrophilic polyvinyl alcohol (PVA) can form chemically and/or physically crosslinked hydrogels. Most PVA hydrogels are biodegradable, highly crystalline, non-toxic, inexpensive, biocompatible, and non-carcinogenic (Asher, Kimble, & Walker, 2008; Kobayashi, Chang, & Oka, 2005; Peresin, Habibi, Vesterinen, et al., 2010). For example, a type of PVA-based hydrogel known as Salubria TM (Salumedic, Atlanta, GA) is marketed in Canada and Europe for articular cartilage replacement (Slaughter, Khurshid, Fisher, Khademhosseini, & Peppas, 2009). However, there are many applications requiring stronger hydrogels (e.g., electrochemical devices and medical implants). To enhance the mechanical strength and toughness of hydrogels, composite hydrogels have been synthesized by incorporating nanoparticles, including carbon nanotubes, metallic particles, and clay (Shin, Spinks, Shin, Kim, & Kim, 2009). These reinforcing nanofillers generally act as decelerators of propagating cracks and contribute to delaying the collapse of the composite hydrogels (Shin et al., 2009). Inspired by the recent environmental concerns, eco-friendly composite hydrogels based on renewable natural resources (e.g., cellulose, most abundant renewable natural biopolymer in nature) have assumed great significance for reinforcing various polymers. Because of the hydrophilic nature of PVA, dispersion of hydrophilic CNPs into the matrix can be readily achieved by blending an aqueous CNP dispersion with an aqueous PVA solution (Paralikara, Simonsen, & Lombardi, 2008). More importantly, cellulose exhibits a low immune response and cannot be degraded and digested in the body due to the fact that human and animal cells do not synthesize the enzymes capable of degrading cellulose (cellulases), thus cellulose reinforced hydrogels are particularly suitable for certain biomedical fields.

* Corresponding author. Tel.: +1 225 578 8369; fax: +1 225 578 4251.
E-mail address: qwu@agcenter.lsu.edu (Q. Wu).

0144-8617/$ – see front matter © 2013 Elsevier Ltd. All rights reserved.
http://dx.doi.org/10.1016/j.carbpol.2013.11.045

In our previous study (Han, Lei, & Wu, 2013), we successfully synthesized PVA-borax hydrogels that were reinforced by well-dispersed cellulose nanoparticles (CNPs). The obtained tough, high-water-capacity (~96%), low-density (~1.1 g/cm^3), translucent hydrogels exhibited birefringence behavior and a higher transparency than the cyclic freeze–thaw prepared opaque hydrogels. Highly crystalline CNPs acted as a multifunctional crosslinking agent to physically and chemically bridge the 3D network hydrogels. By respectively incorporating three types of well-dispersed CNPs to the PVA-borax aqueous system, the mechanical strength, energy absorption and stiffness of the composite hydrogels were significantly enhanced.

Application of the hydrogels in many fields requires a fundamental understanding of their viscoelastic properties. Among those techniques that have been used to investigate the gelation kinetics of PB aqueous system, dynamic rheological techniques have attracted strong interest as a powerful and effective approach to study the supramolecular structure of hydrogels since in situ experiments are relatively facile to perform during the gelation process (Shi et al., 2012). The network structure and the cross-linking density are key factors derived from the rheological characteristics of the hydrogels (Kjøniksen & Nyström, 1996). The linear viscoelastic behavior in dynamic experiments of miscible gelling polymer systems can continuously monitor the development of cross-links (chemical and/or physical) and supramolecular complexes in hydrogel without disrupting gel structure, and they can further reflect the miscibility of polymer blends, supramolecular structure and cross-linking density of hydrogels in stages. As a result, effort has been devoted to the rheology study of PVA-borate complex aqueous systems over the past several decades (Angelova et al., 2011; Carretti et al., 2009). The effects of polymer concentration, molecular weight and temperature on the dynamic viscoelasticity of PVA in aqueous borax solutions were discussed (Koike, Nemoto, Inoue, & Osaki, 1995). The thermo-dynamic, structural, and dynamic features of cross-linked PVA hydrogels and the corresponding semidilute polymer solutions were also reported (Kjøniksen & Nyström, 1996). The crosslinking mechanism of borate ion with PVA chains was known to be a “di-diol” complexation, which was formed between one borate ion and two diol units. PB aqueous system rheologically behaved like elastic solids at high frequencies and like viscous liquids at low frequencies. The short relaxation time and small amount of energy required to break and reform the cross-links accounted for the “slime” consistency of these materials (Angelova et al., 2011). Above-mentioned studies indicate that dynamic rheology techniques can distinguish appropriate gelation conditions for the fabrication of PB hydrogels with desired properties. Regarding the industrial potential in the processing of related materials, the knowledge of the dynamic rheological behavior of PB-based system is very useful in equipment selection and quality control (Gouvea et al., 2009).

However, to the best of our knowledge, we are unaware of any reports on the gelation mechanism and rheological viscoelasticity of PVA-borax-CNP complexes in an aqueous system. For instance, the effects of different CNPs on the rheological features of PB aqueous systems have not been addressed. It is possible that the physically and chemically crosslinked hydrogels can exhibit some unique viscoelastic properties. The objectives of this study were to characterize the dynamic rheological behavior of the obtained hydrogels, and to explore the plausible mechanism for the multi-complexation between CNPs, PVA and borax for a better understanding of the relationship between 3D network structure and hydrogel properties, which could further deepen the fundamental knowledge of how hydrogels were strengthened by CNPs in the presence of borax. Insights into the structural and viscoelastic changes that occurred when the nature of CNPs were changed were obtained from analyses of rheology data. In the work, the effects of particle size, aspect ratio, crystal structure, surface charge and minimum overlap concentration of different CNPs on the dynamic rheological properties and performance of the hydrogels were investigated. Through dynamic oscillation measurements, the enhancement effect of CNPs on the composite hydrogels was verified. Since dynamic bonds formed between the $B(OH)_4^-$ and the OH groups on the sides of the PVA (and/or CNPs) are reversible and exchangeable, the self-healing ability and thermo-reversibility of composite hydrogels were also demonstrated. In addition to providing fundamental insight into factors controlling the efficiency of the cross-links and the interactions among these network components of the composite hydrogels, this work described a new type of soft matter with some unique properties that can be tuned by the incorporation of different CNPs to meet the requirements of specific applications.

2. Experimental

2.1. Materials and hydrogel preparation

Three kinds of CNPs were isolated from bleached wood pulp using alkali pretreatment and/or sulfuric acid hydrolysis followed by a high-pressure homogenization as previously described in our work (Han, Zhou, French, 2013; Han, Zhou, Wu, Liu, & Wu, 2013). The cellulose nanocrystals with I and II crystalline allomorphs as well as the cellulose nanofibers with crystal I structure were designated as CNC I, CNC II and CNF I, respectively. Their corresponding length, width and aspect ratio were 149 ± 40, 46 ± 18 and 732 ± 208 nm; 9 ± 2, 5 ± 1 and 21 ± 7 nm; 16.6, 9.4 and 36.6, respectively (Han, Zhou, Wu, et al., 2013). The obtained CNP aqueous suspensions (1.0 wt%) were stored at 5 °C in a refrigerator before use. As previously described (Han, Lei, & Wu, 2013), dried borax powder (sodium tetraborate decahydrate, over 99.5% purity, $Na_2B_4O_7{\cdot}10H_2O$, $M_w = 381.37$ g mol^{-1}, Aldrich Chemical Co.) was dissolved in 1.0 wt% CNP aqueous suspensions at room temperature to obtain the aqueous solutions with 0.4 wt% of borax. A weighed amount of PVA powder (2.0 wt%) (M_w = 146,000–186,000 g mol^{-1}, 99.0+% hydrolyzed, Aldrich Chemical Co.) was then gently scattered into the stirred aqueous solutions. The mixtures were stirred for 0.5 h at room temperature to prevent the PVA powder from forming lumps and to allow a complete swelling of the PVA chains. Afterwards, the solutions were heated to 90 °C and stirred for 2 h. The heating process was carried out in hermetically sealed flasks to avoid water evaporation and film formation on the surface of the solution. Once the PVA was totally dissolved, homogeneous translucent solutions with well-dispersed CNPs were obtained. The mixture began to exhibit viscoelasticity with the decreasing temperature. The solutions were further cooled to room temperature to form the final hydrogels. All the hydrogels were homogeneous and stable even after they were allowed to stand for more than 8 months at room temperature. Accordingly, the PVA-borax hydrogel was prepared by directly dissolving PVA powder (2.0 wt%) into borax aqueous solutions (0.4 wt%). All other processing conditions were the same as those used for the CNP–PVA-borax hydrogels. On the whole, all the hydrogel samples contained 2.0 wt% of PVA and 0.4 wt% of borax. The hydrogels with 1.0 wt% of CNC I, CNF I and CNC II were designated as PB-CNC I, PB-CNF I and PB-CNC II, respectively, and they were collectively referred to as CNP-reinforced PB hydrogels. The PVA-borax-water complex solution was designated as PB. Deionized water was used for the solution preparation. All solvents and reagents were of analytical grade.

2.2. Dynamic oscillation measurement

The hydrogels (PB, PB-CNC I, PB-CNF I and PB-CNC II) and suspensions (CNCI, CNF I and CNC II at 1.0 wt%) were transferred to

airtight vials to prevent the evaporation of water. They were then allowed to equilibrate for three days for complete structure formation prior to testing. The dynamic rheological behaviors, including dynamic strain sweep, dynamic frequency sweep, continuous step strain and dynamic temperature sweep, were investigated with an AR2000EX controlled-stress Rheometer (TA Instruments Inc., New Castle, DE) using plate-and-plate geometry (diameter 40 mm, gap 500 μm). The upper plate was made of stainless steel, and the lower plate was a Peltier device with a specially designed temperature control system. For each measurement, to minimize shearing during sample loading, approximately 0.6 ml of each sample was carefully loaded onto the Peltier plate using a tablespoon. After their loading, the upper plate was set at a desired distance above the Peltier plate, and then, all samples were equilibrated without pre-shearing or oscillating for 10 min at 25 °C prior to conducting the experiments. To avoid the evaporation of water and the oxygen contamination during measurements, the gap between two plates was sealed with the solvent trap cover, and the moat on the top of the cover was filled with the low viscosity silicon oil.

2.3. Dynamic strain sweep

Before the dynamic viscoelastic measurements, the dynamic strain sweep from 0.01 to 100% at $\omega = 1.0$ Hz was first performed, and the storage modulus was recorded to define the linear viscoelastic region (LVR) in which the storage modulus is independent to the strain amplitude. A strain (γ) of 1.0% was selected in the subsequent oscillation tests to ensure that the dynamic oscillatory deformation of each sample was within the LVR.

2.4. Dynamic frequency sweep

The viscoelastic parameters (log mode), including shear storage modulus (G') and loss modulus (G'') as functions of angular frequency (ω) were measured over the ω range of 0.1–100 rad/s at $\gamma = 1\%$ at 25 °C. The complex modulus (G^*), complex viscosity (η^*), and loss tangent ($\tan\delta$) were calculated by Eqs. (1)–(3), respectively:

$$G^* = \sqrt{G'^2 + G''^2} \tag{1}$$

$$\eta^* = \frac{G*}{\omega} \tag{2}$$

$$\tan\delta = \frac{G''}{G'} \tag{3}$$

2.5. Continuous step strain

To investigate the recovery properties of the hydrogels in response to applied shear forces (expressed in terms of strain), two different 1 h-programmed procedures were used as follows (strain% and duration in parentheses): for PB-CNF I, 1.0% (700 s) → 100% (700 s) → 1.0% (700 s) → 100% (700 s) → 1.0% (800 s); for PB-CNC I, 10% (700 s) → 100% (700 s) → 10% (700 s) → 100% (700 s) → 10% (800 s), and the G' and G'' dependence of time was recorded in continuous step strain measurements at $\omega = 1.0$ Hz and at 25 °C.

2.6. Dynamic temperature sweep

To test the thermo-reversibility by the dynamic temperature sweep, the hydrogel samples were measured through a heating-cooling-heating process (10-70-10-70 °C) at $\omega = 1.0$ Hz and $\gamma = 1.0\%$. The heating and cooling rates were 2.0 and 1.0 °C/min, respectively (Li et al., 2001). Each measurement was repeated three times.

2.7. Wide-angle X-ray diffraction (WXRD)

WXRD patterns of the hydrogel samples were measured using a Bruker/Siemens D5000X-ray automated powder X-ray diffractometer. Before testing, each freeze-dried sample was dried again in a vacuum oven at 60 °C for 24 h to remove moisture. The WXRD data were generated by a diffractometer with Cu Kα radiation ($\lambda = 1.542$ Å) at 40 kV and 30 mA over the angular range $2\theta = 5-40°$, a step size of 0.02°, and a step time of 2.0 s (1.0 h per scan). The data were further smoothed using the MDI Jade 6.5.26 software (Serial No.: MDI-R99691, Materials Data Inc., Livermore, California). The degree of crystallinity or crystallinity index (*CI*, %) for each sample was approximately evaluated using Eq. (4) (Zhang, Zhao, Zhu, He, & Wang, 2012):

$$CI = \left(\frac{A_c}{A_a}\right) \times 100\% \tag{4}$$

where A_c is the area of the crystalline reflection and A_a is the area subtending the whole diffraction profile.

3. Results and discussion

3.1. LVR determined by dynamic strain sweep

Fig. 1a shows the G' as a function of γ for each sample based on the results from dynamic strain sweep tests, demonstrating a typical elastic response of hydrogels. In the dynamic oscillation approach, increasing cyclic levels of γ (from 0.01 to 100%) were applied at $\omega = 1.0$ Hz. Within LVR, the G' values of these hydrogels were basically independent of the applied γ, behaving like a viscoelastic solid. The points at which the G' values deviated by more than 5% from the plateau values indicated departure from linear viscoelastic behavior and therefore were defined as the critical strains (γ_c) for each sample (Gao, Guo, & Nishinari, 2008). The G' values then gradually decreased above the γ_c, indicating a transition of the hydrogel samples from the quasi-solid state to a quasi-liquid state. As shown in Table 1, the γ_c values of PB-CNF I, PB-CNC I and PB-CNC II were 2.0, 3.2 and 31.7%, respectively. Consequently, the $\gamma = 1.0\%$ was selected in the subsequent oscillation tests to ensure that the following dynamic oscillatory deformation of each sample was within LVR. The corresponding G'_{max} were 1715, 1223 and 206 Pa, respectively. As noted from the graph, the three types of CNP-reinforced hydrogels exhibited significantly higher G' values than PB or 1.0 wt% CNP colloids. For example, the G'_{max} of PB-CNF I was two order of magnitude greater than that of PB, and it was also 20 times larger than that of 1.0 wt% CNF I colloid. As expected, the addition of a small amount (1.0 wt%) of CNPs pronouncedly increased the viscoelasticity and stiffness of PB hydrogel. In general, the LVR is shortest when the sample is in its most solid form. Compared with PB-CNC I and PB-CNC II, PB-CNF I present a relatively higher G'_{max}, a shorter LVR and therefore a lower γ_c. This phenomenon indicated that PB-CNF I was the strongest hydrogel.

3.2. Dynamic viscoelasticity of hydrogels

To understand the influence of various CNPs on the viscoelastic properties of hydrogels, oscillatory measurements were carried out at 25 °C in PB-CNC I, PB-CNF I, PB-CNC II and PB hydrogels, as well as the 1.0 wt% cellulose colloidal suspensions (Fig. 1). The G' (elasticity) and G'' (viscosity) as a function of ω for hydrogels within linear deformation range are illustrated in Fig. 1b. It was clearly observed that the G' (ω) or G'' (ω) of these hydrogels essentially followed a similar trend, thus the moduli curves of PB-CNC I were taken as an example to interpret the viscoelastic behavior of hydrogels. At low frequencies where G'' (ω) > G' (ω) ($\tan\delta > 1.0$ in Fig. 1e), quasi-liquid behavior was dominating. As ω proceeded, there was a regional

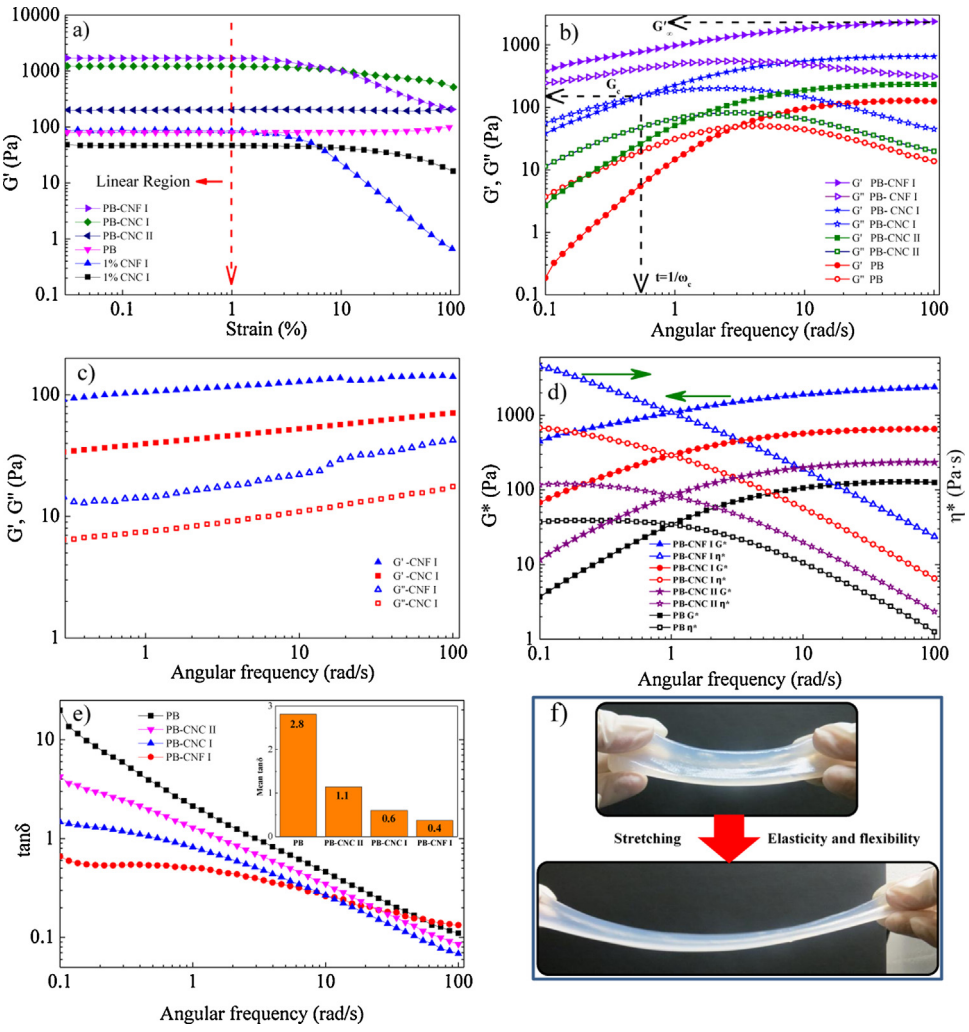

Fig. 1. Dynamic viscoelasticity performance of hydrogels at 25 °C: (a) strain dependence of G' for hydrogels and cellulose colloidal suspensions, measured at $\omega = 1.0$ Hz; (b) frequency dependence of G' and G'' for hydrogels and (c) 1.0 wt% cellulose colloids measured at $\gamma = 1.0\%$; (d) frequency dependence of G^* and η^* for hydrogels; (e) frequency dependence of tan δ for hydrogels; (f) stretching demonstration of PB-CNF I.

monotonic increase in moduli. Simultaneously, $G'(\omega)$ was gradually getting closer to $G''(\omega)$ until a crossover point of $G'(\omega)$ and $G''(\omega)$ curves appeared, suggesting the entanglement of polymer chains and the formation of an elastic gel network (Wang & Chen, 2011). After the crossover point where $G'(\omega) = G''(\omega)$, $G'(\omega)$ continued to increase to reach a plateau region (indicative of polymer entanglements) (Lin, Liu, Yu, Liu, & Rwei, 2005), and it exceeded the $G''(\omega)$ at high frequency range, whereas the curve of $G''(\omega)$ reached its peak and then started to decrease. At high frequencies where $G'(\omega) > G''(\omega)$ ($\tan\delta < 1.0$ in Fig. 1e), the elastic character became the dominant factor, exhibiting a typical solid-like character. These features corresponded to the typical viscoelastic material with a narrow distribution of relaxation times (Inoue & Osaki, 1993). It was noticed that the moduli curves of PB-CNF I only showed the rubbery zone within the accessible frequency window ($\omega = 0.1$–100 rad/s), indicating that their intersection located out of ω window and the gelation occurred at a lower ω, earlier than other samples. According to its viscoelastic properties and the trend of moduli curves of the other gelatinous samples, the crossover point of PB-CNF I was roughly estimated to be at $\omega < 0.1$ where $G'(\omega) = G''(\omega) \approx 246$ Pa. It was generally considered that the presence of crossover between the $G'(\omega)$ and $G''(\omega)$ curves was the sign of gelation (Boluk, Zhao,

Table 1
Rheological characteristics of hydrogels derived from moduli curves.

Parameters	Hydrogels			
	PB	PB-CNC II	PB-CNC I	PB-CNF I
Crossover frequency, ω_c (rad/s)	2.93	1.59	0.54	<0.10
Crossover modulus, G_c (Pa)	48	76	151	~246
Dynamic relaxation time, t (s)	0.34	0.63	1.85	>10.0
High-frequency plateau of G', G'_∞ (Pa)	125	233	652	2356
Maximum G'', G''_m (Pa)	50	83	202	552
Correlated frequency at G''_m, ω_m (rad/s)	3.98	3.42	2.15	2.93
Longest relaxation time, t_L (s)	0.25	0.29	0.47	0.34
Critical strains, γ_c (%)	n.a.	31.7	3.2	2.0
Maximum G' within LVR, G'_{max} (Pa)	80	206	1223	1715

& Incani, 2012), suggesting the formation of the elastic three-dimensional network of both entangled chains and reversible or transient cross-links (Carretti et al., 2009).

Before the incorporation of PVA and borax, G' and G'' curves of 1.0% CNF I colloid and CNC I suspension were relatively independent of ω throughout the whole ω range (Fig. 1c), evidencing the formation of a gel-like transient network structure of entangled nanofibers (Rezayati Charani, Dehghani-Firouzabadi, Afra, & Shakeri, 2013). The slight increase for moduli indicated that the pure cellulose network structure was gradually disequilibrated as shear stress increased, because CNPs were allowed to rearrange and to form an ordered network structure again. G' and G'' curves were almost parallel and G' was one order of magnitude higher than that of G'' at $\omega = 0.1$–100 rad/s, indicating a rather stable and strong networking of the colloid (Wang & Chen, 2011). The G' values of CNF I was nearly one order of magnitude greater than those of CNC I throughout the measured ω window (0.1–100 rad/s), indicating a more gel-like behavior of CNF I colloid due to the inherent entangled 3D networks that were constructed by the higher aspect ratio CNF I (Agoda-Tandjawa et al., 2010; Liu, Chen, Yue, Chen, & Wu, 2011). The other reason was that the critical concentration of CNF I was smaller than that of CNC I, which was detailed in the following mechanism discussion.

Since the non-Newtonian behavior of the CNP-reinforced PB hydrogels, the combination of fluid-like and solid-like properties made them a Maxwell material. Due to a rough approximation to a model with a single Maxwell element (Ivanov, Larsson, Galaev, & Mattiasson, 2004), the hydrogels could be characterized by the following parameters around the crossover coordinates: Crossover modulus (G_c), crossover frequency (ω_c), and dynamic relaxation time (t) of the system (defined as $t = 1/\omega_c$) (Angelova et al., 2011). It was previously reported that the variations in G_c and t represented the changes in the degree and the lifetime of the cross-linking within the hydrogels, respectively (Piculell, Egermayer, & Sjöström, 2003). On the other hand, as noted in Fig. 1b and Table 1, the intersection point (G_c) did not correspond to the maximum value of G'' (ω) for each hydrogel sample, revealing that the viscoelastic properties of the hydrogels should not be described only by one t or by one Maxwell element model (Gao et al., 2008; Koike et al., 1995; Piculell et al., 2003). In other words, even though the single Maxwell element together with the single relaxation time (t) clearly outlined the great differences between different hydrogels, it seemed that a single Maxwell element was no longer enough to describe the behavior of the hydrogels, especially for the PVA-borate-based system (Carretti et al., 2009; Ivanov et al., 2004). Based on Chompff–Duiser theory and modified Rouse theory (Chompff & Prins, 1968), the relaxation spectrum was predicted to illustrate the maximum of characteristic entanglement slipping mechanism. Accordingly, the curve of G'' (ω) should possess a maximum value (G''_m), and that of G' (ω) should have a flat plateau (G'_∞). For this reason, some other characteristic parameters derived from moduli curves could also be used to evaluate the hydrogels in the study: plateau value of G' at high frequencies (G'_∞), the maximum value of G'' (G''_m), correlated frequency ω_m at G''_m and the longest relaxation time t_L (defined as $t_L = 1/\omega_m$). The t_L was described as the time for a given macromolecules to disengage by a snake-like motion from a tube consisted of neighboring polymer chains (Gao et al., 2008). The estimated values of these parameters for the hydrogels in Fig. 4b were given in Table 1.

The most striking difference was observed in G'_∞, which was in the order of PB-CNF I > PB-CNC I > PB-CNC II > PB. For example, with the addition of CNF I, an increase of almost 19-fold in G'_∞ was generated for PB-CNF I compared with pure PB hydrogel, suggesting the cross-link role and enhancement effect of CNPs. On the other hand, the G'_∞ values of PB-CNF I (2356 Pa) and PB-CNC I (652 Pa) were much higher than the G' values of CNF I (141 Pa) and CNC I (70 Pa) colloids at the same cellulose concentration of 1.0 wt% (Fig. 1c), respectively, indicating a strong interaction and entanglement between CNPs and polymer chains. The presence of G'_∞ also indicated that some internal structures might exist, showing the gelation character of the CNPs (Boluk et al., 2012). On the basis of the correlation between entanglement density (ρ_e) and G'_∞ ($G'_\infty = \rho_e k_B T$) (Schubert, Kaler, & Wagner, 2003), the G'_∞ value (a solid-like characteristic) could be used with rubber elasticity theories to estimate the crosslink density. Therefore, the degree of cross-linking by polymer junctions in the cellulose reinforced hydrogels should follow the similar order: PB-CNF I > PB-CNC I > PB-CNC II. Additionally, the crossover modulus (G_c) of these hydrogels, which also provided information about the degree of cross-linking (Carretti et al., 2009), had the same sequence as G'_∞, further confirming the increase in entanglement density from PB to PB-CNF I. This result was further explained by the minimum overlap concentration of CNPs in the mechanism discussion. In addition to the increase in the quantity of cross-links, the increased G'_∞ might also originate in the anionic charges carried by monodiols in the PVA-borax network, thus resulting in a stronger repellence of the polymeric chains (Ivanov et al., 2004).

Consistent with the increase in G'_∞, the relaxation time (t) of the cellulose reinforced hydrogels was considerably extended in the order of PB-CNF I > PB-CNC I > PB-CNC II > PB. Specifically, the t of PB-CNC I was almost 6 times longer than that of neat PB hydrogel, revealing a much slower shear-induced rearrangement of the 3D network and dissociation of cross-links of PB-CNC I under oscillatory shear (Carretti et al., 2009). The relaxation time (t) represented the shape stability of hydrogel. As shown in Fig. 1c, PB-CNF I with longer relaxation time ($t > 10$) could be molded into a more regular cube compared to PB-CNC I ($t = 1.85$) and PB-CNC II ($t = 0.63$), while pure PB hydrogel with a much smaller relaxation time ($t = 0.34$) was not even mouldable. It was generally considered that an increase in t was probably ascribed to a longer lifetime of the cross-links under physical forces, denser polymer entanglements or a higher cross-link density, and the existence of two types of interacting polymer chains slowed down the relaxation process in the hydrogel due to entanglements and different strength of cross-links (Ivanov et al., 2004). It was previously reported that neither borate nor PVA concentration affected the distribution of relaxation times (Robb & Smeulders, 1997). Therefore, different nature of these three kinds of CNPs and their interaction with PVA-borax system were mainly responsible for the different hydrogel properties.

It was also found that the G''_m values of hydrogels were in the same order of PB-CNF I > PB-CNC I >PB-CNC II > PB, which was in an agreement with the results of t and G'_∞. This phenomenon showed the gradual increase in effective degree of crosslinking and chain entanglement from PB ($G''_m = 50$ Pa) to PB-CNF I ($G''_m = 552$ Pa) (Fang, Takahashi, & Nishinari, 2004). The plots of complex modulus (G^*), complex viscosity (η^*) and loss tangent ($\tan\delta$) as a function of ω provided a sharper contrast of these hydrogels (Fig. 1d and e), where PB-CNF I possessed the highest G^* and η^* as well as the smallest $\tan\delta$ within the whole ω range, further confirming that PB-CNF I was the strongest and most elastic hydrogel among these samples. As shown in Fig. 1f, rubbery PB-CNF I could be stretched into a thin film without damage, exhibiting its high elasticity and flexibility. This observation suggested that the hydrogel possessed outstanding damage-tolerant ability and efficient energy dissipation behavior. It is well-known that $\tan\delta$ represents the ratio of dissipated energy to stored energy during the stress deformation. The $\tan\delta$ values of PB-CNF I were lower than 1 throughout the whole ω range (Fig. 1e) and the corresponding mean $\tan\delta$ was 0.4 (insert in Fig. 1e). Because polymer chains physical entanglements were disentangled and then reconstituted during dynamic strains, the dynamic entanglement–disentanglement equilibrium process provided the network with the energy release capacity (Yang et al.,

2012). Their elastomeric nature was probably due to the entanglements of long CNF I and flexible PVA chains via hydrogen bonds and physical junctions with the presence of borax. The homogeneously dispersed CNPs in PVA-borax system were thus regarded as multifunctional cross-links and enhancement fillers.

However, the longest relaxation times (t_L) of hydrogels were in a different order of PB-CNC I > PB-CNF I > PB-CNC II, which was coincident with the sequence of the corresponding Zeta potential (absolute value) of CNC I, CNF I and CNC II (i.e., $|-57.07 \pm 1.06| > |-32.61 \pm 1.12| > |-0.63 \pm 0.08|$ mV) (Han, Zhou, Wu et al., 2013). In our previous work, we mentioned that the negatively charged CNPs electrostatically repulsed each other. Therefore, the highly charged CNC I (zeta potential = -57.07 ± 1.06 mV) increased the organization and the stability of the hydrogel, leading to a longer t_L of PB-CNC I. In the CNP–PVA-borax system, various polymer chains might be reversibly linked to a neighboring chain through crosslinks. During the polymer reptation caused by external oscillatory shear, the exchange rate for the formation of temporarily intermolecular crosslinks was reduced due to a more stable network formed by highly negatively charged fibers. To sum up, these results showed that the incorporation of CNPs significantly increased t, t_L, G'_∞, G''_m and G_c. It was thus concluded that the CNPs strengthened the 3D entangled networks of the PB hydrogels.

3.3. Self-recovery of the hydrogels under continuous step strain

Interestingly, it was noted that these high-water-content hydrogels exhibited particular recovery of their mechanical characteristics after a large-amplitude oscillatory collapse, indicating a thixotropic nature (Wang et al., 2010). As shown in Fig. 2a, beginning to be deformed at small-amplitude oscillatory force ($\gamma = 1.0\%$), PB-CNF I first present a solid nature with a G' of 12.0 KPa and a G'' of 5.1 kPa ($\tan\delta = G''/G' \approx 0.4$). Under the application of a large-amplitude one ($\gamma = 100\%$), the G' and G'' values of PB-CNF I subsequently decreased to 0.23 and 0.7 kPa, respectively, leading to a quasi-liquid state of hydrogel ($\tan\delta \approx 3.0$). However, more importantly, when the γ is reduced once again to 10%, G' and G'' immediately recovers their initial values and the hydrogel returned to the original quasi-solid state ($\tan\delta = 4.5$ kPa/12.2 kPa ≈ 0.4). Accordingly, PB-CNC I showed similar recovery properties in response to applied shear forces, which also experienced the state transition between quasi-liquid ($G'' > G'$ at $\gamma = 100\%$) and quasi-solid ($G'' < G'$ at $\gamma = 10\%$) under oscillatory collapse (Fig. 2b). Nonetheless, under the same oscillatory force (for example, $\gamma = 100\%$), the G' and G'' of PB-CNF I were greater than those of PB-CNC I ($G' \approx 0.14$ kPa, $G'' \approx 0.41$ kPa), confirming that PB-CNF I were more elastic and stronger, which was consistent with the results of compression and dynamic rheology testing.

Because of the reversible cross-links between PVA (or CNPs) and borax, these high-water-content and translucent hydrogels could be manually molded into various 3D shapes (Fig. 2c), suggesting their high malleability and flexibility. In addition, when two blocks of PB-CNF I were pushed together, their surfaces came into adhere to each other, resulting in a fusion phenomenon (Fig. 2d). After readily handling by hand, they could be totally merged together, which was a sign of apparent self-healing property (Schultz & Myers, 1969). This external force-induced coalescence of rubbery hydrogels was probably attributed to their high water content and the hydrophilic nature of polymer chains. To further demonstrate their self-recovery ability, a plastic transfer pipette was inserted into a block of PB-CNF I to create a hollow on the surface of hydrogel (Fig. 2e). As expected, the hollow gradually disappeared under external force, revealing that the flexible hydrogel network could bear strong force and dissipate a large amount of energy without permanent change in 3D-network structure.

3.4. Thermo-reversibility of the hydrogels characterized by temperature sweep

To understand the behavior of hydrogels at different energy states, the CNP reinforced hydrogels were subjected to a temperature sweep study. The junctions of PVA-borate were thermoreversible cross-links with a finite lifetime (determined by oscillation measurement and mechanism section), and some cellulose-based gels also exhibited thermo-reversible characteristic, thus the thermo-reversibility (referred to the reversibility responding to temperature) of these mouldable hydrogels was expected. To test this hypothesis, the hydrogels were developed via a first heating process beginning from a low temperature of 10 °C to 70 °C at a heating rate of 2 °C/min, and were then cooled slowly to 10 °C at a cooling rate of 1.0 °C, and were eventually suffered from a second heating process that was identical to the first one. Fig. 3 shows temperature dependence of moduli (G' and G'') for cellulose reinforced hydrogels under the heating-cooling-heating process (10-70-10-70 °C) at $\omega = 1.0$ Hz and $\gamma = 1.0\%$. It appeared that PB-CNF I, PB-CNC I and PB-CNC II exhibited a similar thermo-behavior, therefore PB-CNF I was taken as an example to demonstrate the thermal-induced transition of hydrogels (Fig. 3a). During the entire heating-cooling-heating circle, G' was throughout higher than G'', indicating the completion of gelation and an elastic hydrogel network.

Starting from 10 to 45 °C in the first heating process, the moduli were roughly independent of temperature, and yet G' decreased very slightly with elevation of temperature, suggesting the stable cross-linking structure and more entanglements between CNPs and polymer chains around room temperature (Shi et al., 2012; Yang et al., 2008). The moduli increased gradually with further increase of temperature from 45 to 70 °C, which might be caused by the formation of a denser network at higher temperatures. Due to the high-water-content nature of the hydrogels ($M_C \approx 96\%$), this phenomenon might be better understood by taking into account the thermal-induced water evaporation inside the hydrogels (Fig. 3d). At higher temperature range from 45 to 70 °C, the concentrations of cellulose and polymer increased due to the inevitable water evaporation of hydrogels, leading to shorter distances between CNPs and/or polymer chains and accordingly a higher cross-linking density of hydrogel structure. In addition to the water evaporation factor, the increased physical cross-linking and more chain entanglements at elevated temperature also contributed to the positive dependence of moduli on the temperature ranging from 45 to 70 °C (known as thermal-induced hardening of hydrogels) (Shi et al., 2012). A similar comportment was previously reported for pure cellulose solution. The cellulose solution exhibited more elastic behavior at high temperature because of the junctions between cellulose chains and the formation of networks (Cai & Zhang, 2006). Consequently, the thermal-induced rheological properties of the CNP reinforced hydrogels were similar to that of the cellulose solution, indicating the homogeneous nature of the hydrogels (Shi et al., 2012). Furthermore, better solubilization of borate ions around 60 °C contributed toward better interaction and complexation (compacter network) inside the hydrogel structure during heating (Gouvea et al., 2009).

At the lower temperature range from 10 to 45 °C, the thermal-induced water evaporation was quit slow and even negligible, so the moduli showed almost no dependence on temperature in this range. For the following cooling process, the moduli increased rapidly from 70 to 45 °C, and the ascent rate of moduli was much greater compared to the descent rate of moduli within the same temperature range in the first heating process, which was probably due to the continuous and intense evaporation at higher temperature. Subsequently, at lower temperature range from 45 to 10 °C, the moduli reached a temperature-independent

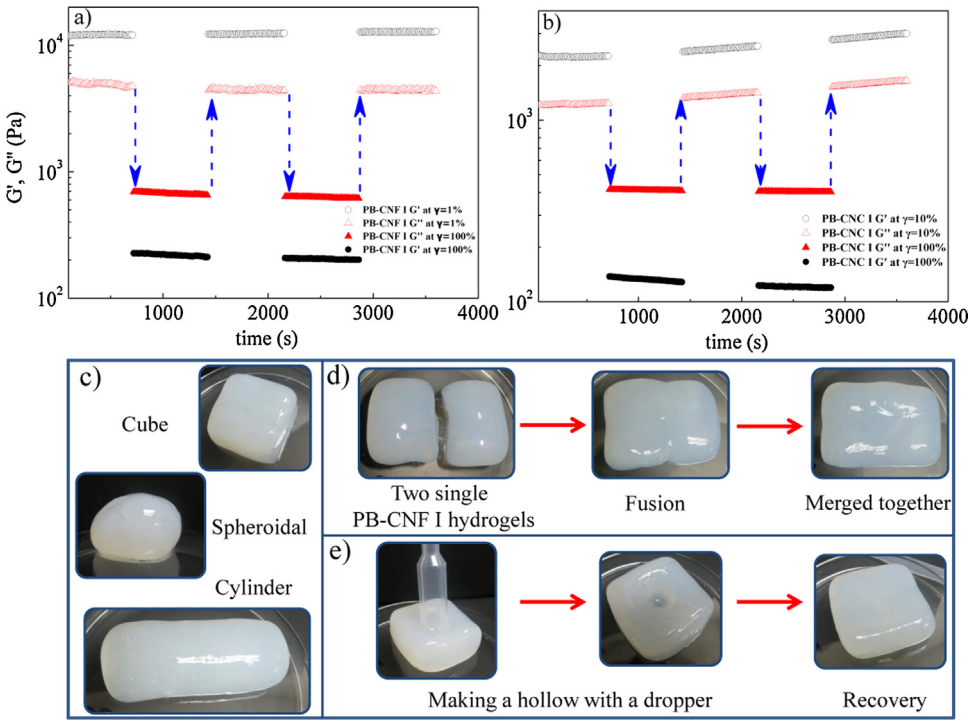

Fig. 2. The G' and G'' dependence of time in continuous step strain measurements for PB-CNF I (a) and PB-CNC I (b); shape-persistent, free-standing macroscopic objects molded from a PB-CNF I hydrogel (c); process of merging two single PB-CNF I hydrogels together (d); the demonstration of shape recovery for PB-CNF I (e).

plateau, suggesting that the temperature region between 10 and 45 °C was indeed suitable to test the thermo-reversibility. Because the thermo-reversibility of a hydrogel is an important characteristic that is directly related to the energy involved in the hydrogel network structure (Gao et al., 2008; Li et al., 2001), the thermal-induced water evaporation will affect the thermal-induced behavior, especially for a high-water-content hydrogel. For this reason, the thermo-reversibility of a hydrogel makes sense only when the water evaporation can be practically ignored. To verify the thermo-reversibility, the hydrogels experienced the second heating process. At lower temperature range from 10 to 45 °C where water evaporation of hydrogels was almost negligible (confirmed by first heating process), the moduli curve of the second heating process basically overlapped the cooling curve, revealing

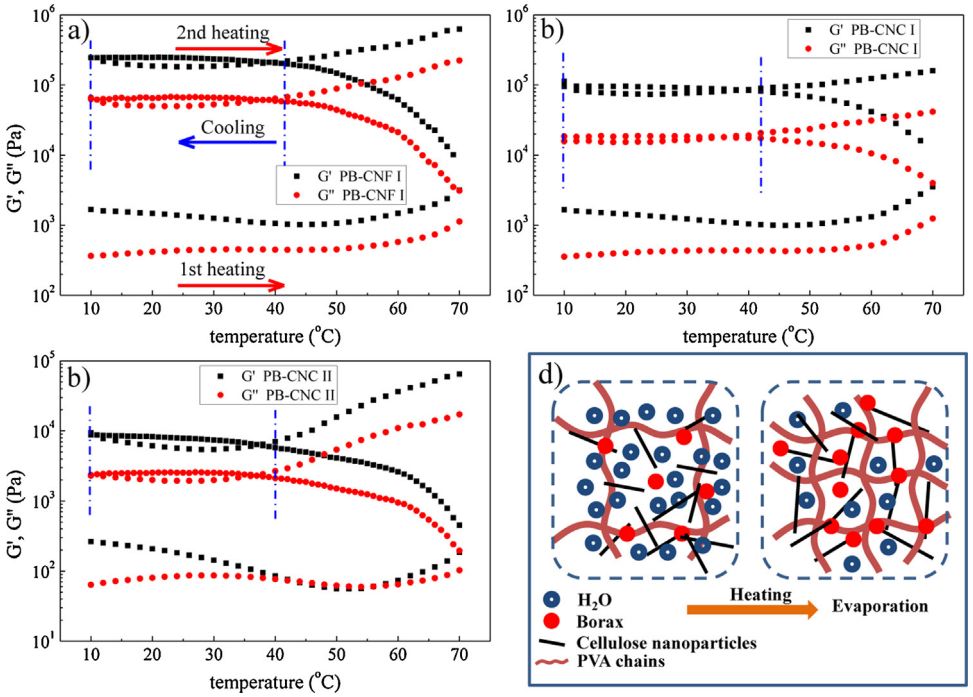

Fig. 3. Temperature dependence of G' and G'' for PB-CNF I (a), PB-CNC I (b) and PB-CNC II (c) during a heating-cooling-heating circle (10-70-10-70 °C) at $\omega = 1.0$ Hz and $\gamma = 1.0\%$, and mechanism of thermo-reversibility (d).

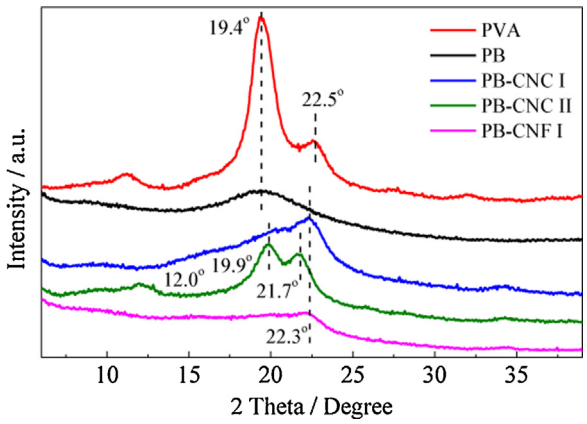

Fig. 4. X-ray diffraction patterns of pure PVA and composite hydrogels.

that hydrogels stiffening during cooling was almost completely thermo-reversible (Renkema & van Vliet, 2002). While at higher temperature range from 45 to 70 °C where water evaporation of hydrogels became more intensified (determined by first heating process), the moduli curve rose again with the same ascent rate as the first heating process. Similar thermo-reversibility of the hydrogels prepared by related polymers was proposed previously, such as glucomannan/borax gel (Gao et al., 2008), short-chain O-(2,3-dihydroxypropyl) cellulose/borax hydrogel (Ide, Sato, Miyamoto, & Fukuda, 1998), and crystalline colloidal array embedded PVA hydrogel (Asher et al., 2008).

3.5. WXRD analysis

The WXRD profiles of pure PVA and composite hydrogels are presented in Fig. 4. Neat PVA exhibited two obvious diffraction peaks at 19.4° and 22.5°, which corresponded to the orthorhombic lattice structure of semi-crystalline PVA (Chen, Cao, Chang, & Huneault, 2008). Note that the addition of borax, the diffraction peaks of PB became weaker and the *CI* of PVA decreased from 43 to 26%. This phenomenon could be explained by that in the PB hydrogel, borax strongly interacted with the hydroxide radical of PVA, and the complexation between them destroyed the organized arrangement of PVA, and in turn reduced the *CI*. For a simple mixture of PVA and CNPs, each component should theoretically have its own crystal peaks in the hydrogels. However, after the CNPs were incorporated into the PB system, the diffraction peak of PB at $2\theta = 19.4°$ disappeared and some new superposition peaks formed. This result suggested that CNPs and PB had good compatibility, leading to the formation of a 3D-network within the composite hydrogels. Our previous study reported that CNF I and CNC I with a crystallographic form of cellulose I exhibited a sharp high peak at $2\theta = 22.6°$ and two overlapped weaker diffraction peaks at $2\theta = 15.1°$ and 16.6°, assigned to (0 0 2), (1 0 1), and (1 0 $\bar{1}$) planes, while CNF II with a crystallographic form of cellulose II had three peaks located at $2\theta = 12.4°$ (1 $\bar{1}$ 0), 20.1° (1 1 0), and 22.1° (2 0 0) (Han, Zhou, Wu, et al., 2013). On the whole, the XRD pattern of PB-CNC I was very close to that of PB-CNF I. As it can be observed, PB-CNC I and PB-CNF I both exhibited broad diffraction peaks at $2\theta = 22.3°$ and thus had a crystalline structure. With the addition of CNC I or CNF I, the *CI* values of PB hydrogel increased from 26 to 54 and 48%, respectively. PB-CNC II showed three peaks at $2\theta = 12.0°$, 19.9°, and 21.7° and its *CI* was increased to 52%. It was thus concluded that the presence of PVA and borax had no effect on the cellulose crystal structure of composite hydrogels, and the *CI* of PB hydrogel was significantly increased with the addition of highly crystalline CNPs. In addition, it was worth noting that the *CI* values of these composite hydrogels (48–54%) were less than those of pure CNPs (66–74%) (Han, Zhou, Wu, et al., 2013), indicating that the crystalline of CNPs was partly prohibited by the strong interaction and complexation between the CNPs and the PB matrix (Chen et al., 2008).

3.6. Possible mechanism for hydrogel formation and CNP enhancement

In order to improve the existing models of PVA-borax gelation to the field of CNP-containing PB hydrogels, it was necessary to consider the fundamentals of PVA-borate complex formation in water. Previous studies elucidated that, in dilute solution (borax concentration less than 25 mM ≈ 0.95 wt%), borax ($Na_2B_4O_7{\cdot}10H_2O$) dissociated completely into equal quantities of trigonal planar [$B(OH)_3$] (boric acid) and tetrahedral [$B(OH)_4^-$] (monoborate ions) that interchanged rapidly in water system (see Eq. (5)) (Cui, Muscatello, & Asher, 2009; Lin, Yu, & Cheng, 2000; Pezron, Ricard, Lafuma, & Audebert, 1988; Sinton, 1987), thus the authentic concentration of $B(OH)_4^-$ in the system was almost twice the initial borax concentration (Gao et al., 2008).

$$Na_2B_4O_7 + 7H_2O \rightarrow 2B(OH)_3 + 2B(OH)_4^- \quad (5)$$

Cellulose, $(C_6H_{10}O_5)_n$, was a polyhydroxy polysaccharide consisting of a linear chain of thousands of β(1 → 4) linked D-glucose units. PVA was a long chain polymer that had a backbone of carbon molecules with numerous 1,3-cis-diol groups attached. In general, the mechanism of the crosslinking reaction of $B(OH)_4^-$ with polyhydroxy polymers (i.e., PVA and cellulose in this study) was considered to be a so-called monodiol and didiol complexation (crosslink reaction) formed between vicinal diol units of polymer chains and $B(OH)_4^-$ (see Eqs. (6) and (7)) (Angelova et al., 2011).

$$P + B(OH)_4^- \leftrightarrow PB(OH)_4^- + 2H_2O \quad (6)$$

$$2P + B(OH)_4^- \leftrightarrow P_2B(OH)_4^- + 4H_2O \quad (7)$$

where P referred to the cis-diol unit of the polymer (cellulose or PVA). $PB(OH)^-{}_4$ (complex I) and $P_2B(OH)^-{}_4$ (complex II) represented the free monodiol (1:1 stoichiometry) and didiol (2:1 stoichiometry) complex structures, respectively.

These complexes played the role of tie points for the physical network. Once a $B(OH)^-{}_4$ was attached to a PVA or cellulose chain (complex I), the anionic polymer chain behaved as a polyelectrolyte unless the $B(OH)^-{}_4$ was removed from it. In this case, a contribution of electrostatic repulsion between monodiol units was expected, leading to an expansion of the individual polymer chains (Lin et al., 2005). Since the PVA concentration (2.0 wt%) in each hydrogel was higher than the overlap concentration C* (1.54 wt%), both intra- and inter-molecular crosslink of (complex II) happened, and a gelation of these complexes was expected.

Based on the above-mentioned analysis, we first realized the multi-complexation between CNPs, PVA and borax in aqueous system in the present study. A plausible mechanism for the multi-complexation between cis-diol groups on the CNPs (or PVA) and $B(OH)^-{}_4$ is presented in Scheme 1. PVA-borax aqueous system had a strong extended H-bonding network, which could further interact with active hydroxyl groups of cellulose through H-bonding. This was the first hierarchy of the hydrogel 3D-network via polymer-chain physical entanglement. It was reported that borate ions preferred to complex with glucose rather than physical cross-linking with the PVA polymer via hydrogen bonding (Manna & Patil, 2010). However, because the chain excluded volume of CNPs was much greater than that of glucose molecules, thus considering the presence of stereo-hindrance effect of the larger CNPs in the medium, the competitive binding equilibrium between PVA and CNPs was mitigated, which meant that the partial

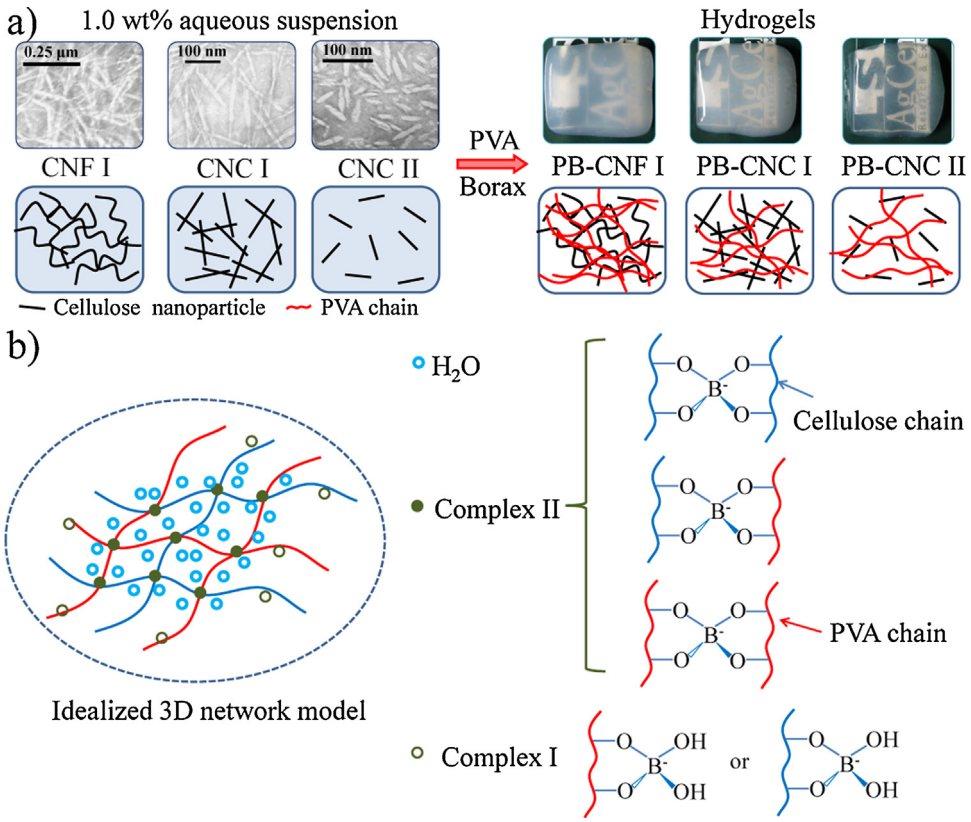

Scheme 1. Schematic illustration of the three-dimensional network formation of hydrogel. (a) The first physical hierarchy of physical entanglement of polymer chains through H-bond, and the comparison of the dispersion state of cellulose nanoparticles with different minimum overlap concentration in the hydrogels, and (b) the second chemical hierarchy of the idealized 3D network structure formed by the ionic crosslinks among the five types of complexes and adjacent water molecules (hydrogen bond system was not shown).

PVA-borax complexes would probably still exist with the addition of CNPs. Therefore, two cis-diol pairs of different cellulose molecules or PVA chains were connected by a $B(OH)_4^-$ to form an reversible inter-chain crosslink. The coexistence of the three types of reversible crosslinks (PVA-$B(OH)_4^-$-CNP, PVA-$B(OH)_4^-$-PVA and CNP-$B(OH)_4^-$-CNP) gave rise to five types of complexes, namely complex I (PVA-$B(OH)_4^-$ and CNP-$B(OH)_4^-$) and complex II (PVA-$B(OH)_4^-$-CNP, PVA-$B(OH)_4^-$-PVA and CNP-$B(OH)_4^-$-CNP), leading to the creation of a tridimensional network and solid-like performance of hydrogels (Scheme 1b). This was the second chemical hierarchy of the hydrogel 3D-network via plenty of reversible ionic crosslinks.

The formation of cross-links between pairs of vicinal hydroxyl groups from two polymer chains (PVA or CNP) and one $B(OH)_4^-$ (Eq. (7)) was an exothermic process, and the cross-linking caused by formation of anionic complexes II with 2:1 stoichiometry was cited as the chemical basis of enhanced viscosification in the system (Robb & Smeulders, 1997; Sinton, 1987). These negatively charged complexes and CNPs as well as free $B(OH)_4^-$ provided the electrostatic repulsion for the system (Manna & Patil, 2009), resulting in the homogeneous dispersion state of these components in hydrogels. In addition to the ionic bonding by borax, PVA chains and CNPs could be cross-linked through hydrogen bonding and van der Waals type of interaction with the presence of water molecules, leading to the intra- and intermolecular cross-linking reactions and thus a physical entanglement (the first physical hierarchy). Consequently, the high-water-content mouldable hydrogel introduced by the present study was defined as the system formed when natural macromolecule (i.e., CNPs) and synthetic polymer (i.e., PVA) were physically entangled and chemically cross-linked with each other via the comprehensive cooperation of ionic bonding (offered by borax), hydrogen bonding and physical entanglement, which could entrap a big volume of water (Gao et al., 2008; Li et al., 2001). In other words, the conformation of the 3D-network polymer chains in these hydrogels was a consequence of a balance among physical entanglement via hydrogen bonding, intra- and intermolecular cross-linking effects, electrostatic repulsions between the complex units, the polymer-chain excluded volume and the electrostatic shielding effect of free Na^+ ions on the negatively charged complexes (Angelova et al., 2011). In addition, it was reported that $B(OH)_3$ had a similar tendency to form diol complexes in the presence of PVA and cellulose. Nonetheless, $B(OH)_3$ hardly contributed to the formation of polyol gels, because the complexation reaction happened through the attachment of $B(OH)_3$ to adjacent alcohol groups of the same polymeric chain, which prevented cross-linking from taking place.

As described in dynamic oscillation measurements, the well-dispersed CNPs played an important multifunctional role on the 3D-network formation within the hydrogels, leading to a significant enhancement in toughness and viscoelasticity of the hydrogels. Before the combination, the PVA-borax-water system was not free-standing; and the 1.0 wt% CNP suspension or colloid was free-flowing. While after the incorporation of rigid CNPs, the crosslinking and entanglement restricted the segmental motions of PVA chains and CNPs, thus the system gradually solidified as temperature decreased and eventually formed a rubbery semisolid hydrogel that was easy to handle and mold at room temperature (Figs. 1f and 2c). Our previous study determined that the crystallinities of CNC I, CNF I and CNC II (66.4, 57.6 and 73.6%, respectively) were greater than that of PVA (43%) (Han, Zhou, Wu, et al., 2013; Peresin, Habibi, Zoppe, Pawlak, & Rojas, 2010). Therefore, the incorporation of highly crystalline CNPs into a softer chain

PVA matrix with a lower degree of crystallinity led to a significant hardening effect. Additionally, the elastic modulus of the crystalline regions of cellulose I (138.0 GPa) was larger than that of cellulose II (88.0 GPa) in the direction parallel to the chain axis (Nishino, Takano, & Nakamae, 1995), making cellulose I reinforced hydrogel absorb more energy under deformation than cellulose II reinforced hydrogel. Overall, the viscoelasticity and mechanical property of the hydrogels were in the order of PB-CNF I > PB-CNC I > PB-CNC II > PB, while their transparency was sequenced in a reverse order (Han, Lei, et al., 2013). As determined by UV-transmittance, rheology and compression data (Han, Lei, et al., 2013), the differences in the enhancement effect and transparency originated in different nature of CNPs, such as aspect ratio, particle size, crystal structure, degree of crystallinity and surface charge. More importantly, for the three types of CNPs, this phenomenon could be further explained based on the understanding of the minimum overlap concentration and the supramolecular structures of these hydrogels.

The minimum overlap concentration (ϕ_c) for dispersions of rod-like CNPs can be approximated by the equation: $\phi_c = (D/L)^2$, where ϕ_c is the minimum overlap concentration in terms of volume fraction, L is the length and D is the diameter of cellulose rods (Bercea & Navard, 2000). The ϕ_c values of CNF I, CNC I and CNC II were estimated to be 0.075, 0.363, 1.130 vol%, respectively. Based on the densities of CNPs (~1.59 g/cm^3) and deionized water (~1.00 g/cm^3) (OSullivan, 1997), their corresponding mass concentrations were calculated. For CNC I suspension and CNF I colloid, the concentration of 1.00 wt% was above their corresponding ϕ_c values, 0.58 and 0.12 wt%, respectively, whereas the ϕ_c value of CNC II suspension was 1.80 wt%, higher than the concentration of 1.00 wt% used in this experiment. Accordingly, as demonstrated in the TEM images (Scheme 1a), at the 1.00 wt% concentration level, long-curved CNF I chains achieved the entanglement, and needle-like CNC I possessed overlap junctions, while rod-like CNC II hardly contacted with each other and thus its inter-particle interactions were almost negligible. In particular, the pronounced entanglement of CNF I chains increased the probability that PVA chains contacted and tangled with CNF I chains, i.e., leading to the formation of physical junctions via polymer chain entanglements (Scheme 1a). On the contrary, the quantity of junction zones of CNC II was much less than those of CNF I and CNC I, especially for the physical junctions formed by its self-entanglement (Scheme 1a). For this reason, the cross-linking (entanglement) densities of hydrogels should be theoretically in the order of PB-CNF I > PB-CNC I > PB-CNC II, which was in agreement with the G'_∞, G_c and t (relaxation time) results of oscillation test. After the cross-linking density was increased by the embedding of CNPs in PB system, plenty of water molecules became trapped inside the 3D network through hydrogen bond due to the hydrophilic nature of PVA and cellulose chains, thus producing a high-water-content hydrogel.

Once prepared, the hydrogels displayed some intriguing properties due to their supermolecular structure. The spaghetti-strand polymer chains gave the hydrogels a non-Newtonian fluid behavior. Under low stress, they could be stretched to form a thin film (Fig. 1f). When a block of hydrogel was thrown onto a hard surface, it bounced slightly. The $B(OH)_4^-$ ion was shaped like a tetrahedron (four sides, each side is an equilateral triangle) with the boron in the center and the four OH groups at each corner. The temporary bonds formed between the $B(OH)_4^-$ and the OH groups on the sides of the PVA were reversible and exchangeable, which was previously confirmed by ^{11}B NMR investigations (Sinton, 1987). The breaking and reformation of these bonds allowed the hydrogel to stretch under stress. The most abundant material in the hydrogels was water ($M_c \approx 96$ wt%), providing the liquid consistency of hydrogels. Therefore, two blocks of hydrogels could be completely merged into a single piece (Fig. 2d). The uncommon fusion behavior of two separated PB-CNF I samples also suggested that the networks were in dynamic equilibrium and that the cross-linkages were not covalent. The ease of bonds break and reform resulted in the hydrogel rebuilt. Because all of the interactions were non-covalent, the constantly forming and dissociating of hydrogen bonds endowed the crosslinks with a dynamic nature, which allowed the PVA chains and CNPs to move relative to each other under external force. Hence these hydrogels could be manually molded into various 3D shapes (Fig. 2c). It was proposed that the activation energy for breaking the four bonds constituting individual cross-links was 25 kJ/mol, while the heat of cross-link formation was 35 kJ/mol (Angelova et al., 2011). Responding accordingly to the external stimuli such as external force and temperature, the hydrogel exhibited self-healing ability and thermo-reversibility (determined by continuous step strain and temperature sweep tests). The PB-CNF I distorted under external force and then gradually wriggled back to its original shape (Fig. 2e). This meant that the tangled PVA chains and CNPs were straighten out and then wriggled to become shorter again.

4. Conclusions

A new class of CNP-reinforced PVA-borax hydrogels was successfully fabricated through a facile approach in an aqueous medium. By respectively incorporating three types of well-dispersed CNPs (i.e., CNC I, CNC II and CNF I) to the PB aqueous system, the viscoelasticity, strength and stiffness of the hybrid hydrogels were pronouncedly enhanced. Highly crystalline CNPs acted as multifunctional crosslinking agents and nanofillers to physically and chemically bridge the double-hierarchy 3D network of the hydrogels, clearly demonstrating the synergy between natural CNPs and synthetic polymer matrix. The nature of the CNPs (i.e., particle size, aspect ratio, crystal structure, and surface charge) affected the dynamic rheological properties of the composite hydrogels. The crosslinking density, viscoelasticity, stiffness of the obtained hydrogels were in the order of PB-CNF I > PB-CNC I > PB-CNC II > PB. Due to the reversible and exchangeable bonds dynamically formed between the $B(OH)_4^-$ and the OH groups on the sides of the PVA (and/or CNPs), the as-prepared free-standing, high elasticity and mouldable hydrogels exhibited self-recovery under continuous step strain and thermo-reversibility under temperature sweep. This novel material is not only environmentally friendly, but is mouldable into various free-standing 3D shapes as well because of its high mechanical strength. In addition, the architectures and properties of hydrogels can be easily tailored by selecting different CNPs and crosslinking density. Our hydrogel contradicts the preconception that materials held together by supramolecular forces and mostly composed of water are weak (Wang et al., 2010), opening the door for many interesting applications, including artificial muscles, bioactuators, soft machines, tissue scaffolds and drug-delivery devices (Calvert, 2009; Hu, Lu, Gao, & Wang, 2000; Seliktar, 2012; Vlierberghe, Dubruel, & Schacht, 2011).

Acknowledgments

The authors are thankful for the financial support fromLouisiana Board of Regents [LEQSF-EPS(2013)-PFUND-318 and (LEQSF(2010-13)-RD-B-01), as well as Chinese Scholarship Council (CSC No.: 2009660015). The author would like to thank Dr. Alfred D. French for valuable discussion on XRD data analysis.

References

Agoda-Tandjawa, G., Durand, S., Berot, S., Blassel, C., Gaillard, C., Garnier, C., et al. (2010). Rheological characterization of microfibrillated cellulose suspensions after freezing. *Carbohydrate Polymers*, *80*(3), 677–686.

Angelova, L. V., Terech, P., Natali, I., Dei, L., Carretti, E., & Weiss, R. G. (2011). Cosolvent gel-like materials from partially hydrolyzed poly(vinyl acetate)s and borax. *Langmuir*, *27*(18), 11671–11682.

Asher, S. A., Kimble, K. W., & Walker, J. P. (2008). Enabling thermoreversible physically cross-linked polymerized colloidal array photonic crystals. *Chemistry of Materials*, *20*(24), 7501–7509.

Bercea, M., & Navard, P. (2000). Shear dynamics of aqueous suspensions of cellulose whiskers. *Macromolecules*, *33*(16), 6011–6016.

Boluk, Y., Zhao, L. Y., & Incani, V. (2012). Dispersions of nanocrystalline cellulose in aqueous polymer solutions: Structure formation of colloidal rods. *Langmuir*, *28*(14), 6114–6123.

Cai, J., & Zhang, L. (2006). Unique gelation behavior of cellulose in NaOH/urea aqueous solution. *Biomacromolecules*, *7*(1), 183–189.

Calvert, P. (2009). Hydrogels for soft machines. *Advanced Materials*, *21*(7), 743–756.

Carretti, E., Grassi, S., Cossalter, M., Natali, I., Caminati, G., Weiss, R. G., et al. (2009). Poly(vinyl alcohol)-borate hydro/cosolvent gels: Viscoelastic properties, solubilizing power, and application to art conservation. *Langmuir*, *25*(15), 8656–8662.

Chen, Y., Cao, X., Chang, P. R., & Huneault, M. A. (2008). Comparative study on the films of poly(vinyl alcohol)/pea starch nanocrystals and poly(vinyl alcohol)/native pea starch. *Carbohydrate Polymers*, *73*(1), 8–17.

Chompff, A. J., & Prins, W. (1968). Viscoelasticity of networks consisting of crosslinked or entangled macromolecules. 2. Verification of theory for entanglement networks. *Journal of Chemical Physics*, *48*(1), 235–243.

Cui, Q., Muscatello, M. M. W., & Asher, S. A. (2009). Photonic crystal borax competitive binding carbohydrate sensing motif. *Analyst*, *134*(5), 875–880.

Fang, Y. P., Takahashi, R., & Nishinari, K. (2004). A gel network constituted by rigid schizophyllan chains and nonpermanent cross-links. *Biomacromolecules*, *5*(1), 126–136.

Gao, S. J., Guo, J. M., & Nishinari, K. (2008). Thermoreversible konjac glucomannan gel crosslinked by borax. *Carbohydrate Polymers*, *72*(2), 315–325.

Gouvea, M. R., Ribeiro, C., de Souza, C. F., Marvila-Oliveira, I., Lucyszyn, N., & Sierakowski, M. R. (2009). Rheological behavior of borate complex and polysaccharides. *Materials Science & Engineering C: Biomimetic and Supramolecular Systems*, *29*(2), 607–612.

Han, J. Q., Zhou, C. J., French, A. D., Han, G. P., & Wu, Q. L. (2013). Characterization of cellulose II nanoparticles regenerated from 1-butyl-3-methylimidazolium chloride. *Carbohydrate Polymers*, *94*(2), 773–781.

Han, J. Q., Zhou, C. J., Wu, Y. Q., Liu, F. Y., & Wu, Q. L. (2013). Self-assembling behavior of cellulose nanoparticles during freeze-drying: Effect of suspension concentration, particle size, crystal structure, and surface charge. *Biomacromolecules*, *14*(5), 1529–1540.

Han, J. Q., Lei, T. Z., & Wu, Q. L. (2013). Facile preparation of mouldable polyvinyl alcohol-borax hydrogels reinforced by well-dispersed cellulose nanoparticles: Physical, viscoelastic and mechanical properties. *Cellulose*, *20*(6), 2947–2958.

Hu, Z. B., Lu, X. H., Gao, J., & Wang, C. J. (2000). Polymer gel nanoparticle networks. *Advanced Materials*, *12*(16), 1173–1176.

Ide, N., Sato, T., Miyamoto, T., & Fukuda, T. (1998). Thermoreversible hydrogel of short-chain O-(2,3-dihydroxypropyl)cellulose/borax aqueous solution. Microscopic versus macroscopic properties. *Macromolecules*, *31*(25), 8878–8885.

Inoue, T., & Osaki, K. (1993). Rheological properties of poly(vinyl alcohol)/sodium borate aqueous-solutions. *Rheologica Acta*, *32*(6), 550–555.

Ivanov, A. E., Larsson, H., Galaev, I. Y., & Mattiasson, B. (2004). Synthesis of boronate-containing copolymers of N,N-dimethylacrylamide, their interaction with poly(vinyl alcohol) and rheological behaviour of the gels. *Polymer*, *45*(8), 2495–2505.

Kjøniksen, A.-L., & Nyström, B. (1996). Effects of polymer concentration and crosslinking density on rheology of chemically cross-linked poly(vinyl alcohol) near the gelation threshold. *Macromolecules*, *29*(15), 5215–5222.

Kobayashi, M., Chang, Y. S., & Oka, M. (2005). A two year in vivo study of polyvinyl alcohol-hydrogel (PVA-H) artificial meniscus. *Biomaterials*, *26*(16), 3243–3248.

Koike, A., Nemoto, N., Inoue, T., & Osaki, K. (1995). Dynamic light-scattering and dynamic viscoelasticity of poly(vinyl alcohol) in aqueous borax solutions. 1. Concentration-effect. *Macromolecules*, *28*(7), 2339–2344.

Li, L., Thangamathesvaran, P. M., Yue, C. Y., Tam, K. C., Hu, X., & Lam, Y. C. (2001). Gel network structure of methylcellulose in water. *Langmuir*, *17*(26), 8062–8068.

Lin, H. L., Liu, Y. F., Yu, T. L., Liu, W. H., & Rwei, S. P. (2005). Light scattering and viscoelasticity study of poly(vinyl alcohol)-borax aqueous solutions and gels. *Polymer*, *46*(15), 5541–5549.

Lin, H. L., Yu, T. L., & Cheng, C. H. (2000). Reentrant behavior of poly(vinyl alcohol)-borax semidilute aqueous solutions. *Colloid and Polymer Science*, *278*(3), 187–194.

Liu, D. G., Chen, X. Y., Yue, Y. Y., Chen, M. D., & Wu, Q. L. (2011). Structure and rheology of nanocrystalline cellulose. *Carbohydrate Polymers*, *84*(1), 316–322.

Manna, U., & Patil, S. (2009). Borax mediated layer-by-layer self-assembly of neutral poly(vinyl alcohol) and chitosan. *Journal of Physical Chemistry B*, *113*(27), 9137–9142.

Manna, U., & Patil, S. (2010). Glucose-triggered drug delivery from borate mediated layer-by-layer self-assembly. *ACS Applied Materials & Interfaces*, *2*(5), 1521–1527.

Nishino, T., Takano, K., & Nakamae, K. (1995). Elastic-modulus of the crystalline regions of cellulose polymorphs. *Journal of Polymer Science Part B: Polymer Physics*, *33*(11), 1647–1651.

OSullivan, A. C. (1997). Cellulose: The structure slowly unravels. *Cellulose*, *4*(3), 173–207.

Paralikara, S. A., Simonsen, J., & Lombardi, J. (2008). Poly(vinyl alcohol)/cellulose nanocrystal barrier membranes. *Journal of Membrane Science*, *320*(1–2), 248–258.

Peresin, M. S., Habibi, Y., Vesterinen, A. H., Rojas, O. J., Pawlak, J. J., & Seppala, J. V. (2010). Effect of moisture on electrospun nanofiber composites of poly(vinyl alcohol) and cellulose nanocrystals. *Biomacromolecules*, *11*(9), 2471–2477.

Peresin, M. S., Habibi, Y., Zoppe, J. O., Pawlak, J. J., & Rojas, O. J. (2010). Nanofiber composites of polyvinyl alcohol and cellulose nanocrystals: Manufacture and characterization. *Biomacromolecules*, *11*(3), 674–681.

Pezron, E., Ricard, A., Lafuma, F., & Audebert, R. (1988). Reversible gel formation induced by ion complexation. 1. Borax galactomannan interactions. *Macromolecules*, *21*(4), 1121–1125.

Piculell, L., Egermayer, M., & Sjöström, J. (2003). Rheology of mixed solutions of an associating polymer with a surfactant. Why are different surfactants different? *Langmuir*, *19*(9), 3643–3649.

Renkema, J. M. S., & van Vliet, T. (2002). Heat-induced gel formation by soy proteins at neutral pH. *Journal of Agricultural and Food Chemistry*, *50*(6), 1569–1573.

Rezayati Charani, P., Dehghani-Firouzabadi, M., Afra, E., & Shakeri, A. (2013). Rheological characterization of high concentrated MFC gel from kenaf unbleached pulp. *Cellulose*, *20*(2), 727–740.

Robb, I. D., & Smeulders, J. B. A. F. (1997). The rheological properties of weak gels of poly(vinyl alcohol) and sodium borate. *Polymer*, *38*(9), 2165–2169.

Schubert, B. A., Kaler, E. W., & Wagner, N. J. (2003). The microstructure and rheology of mixed cationic/anionic wormlike micelles. *Langmuir*, *19*(10), 4079–4089.

Schultz, R. K., & Myers, R. R. (1969). The chemorheology of poly(vinyl alcohol)-borate gels. *Macromolecules*, *2*(3), 281–285.

Seliktar, D. (2012). Designing cell-compatible hydrogels for biomedical applications. *Science*, *336*(6085), 1124–1128.

Shi, X. W., Lu, A., Cai, J., Zhang, L. N., Zhang, H. M., Li, J., et al. (2012). Rheological behaviors and miscibility of mixture solution of polyaniline and cellulose dissolved in an aqueous system. *Biomacromolecules*, *13*(8), 2370–2378.

Shin, M. K., Spinks, G. M., Shin, S. R., Kim, S. I., & Kim, S. J. (2009). Nanocomposite hydrogel with high toughness for bioactuators. *Advanced Materials*, *21*(17), 1712–1715.

Sinton, S. W. (1987). Complexation chemistry of sodium borate with poly(vinyl alcohol) and small diols: A boron-11 NMR study. *Macromolecules*, *20*(10), 2430–2441.

Slaughter, B. V., Khurshid, S. S., Fisher, O. Z., Khademhosseini, A., & Peppas, N. A. (2009). Hydrogels in regenerative medicine. *Advanced Materials*, *21*(32–33), 3307–3329.

Sun, J. Y., Zhao, X. H., Illeperuma, W. R. K., Chaudhuri, O., Oh, K. H., Mooney, D. J., et al. (2012). Highly stretchable and tough hydrogels. *Nature*, *489*(7414), 133–136.

Van Vlierberghe, S., Dubruel, P., & Schacht, E. (2011). Biopolymer-based hydrogels as scaffolds for tissue engineering applications: A review. *Biomacromolecules*, *12*(5), 1387–1408.

Wang, Q., Mynar, J. L., Yoshida, M., Lee, E., Lee, M., Okuro, K., et al. (2010). High-water-content mouldable hydrogels by mixing clay and a dendritic molecular binder. *Nature*, *463*(7279), 339–343.

Wang, Y. X., & Chen, L. Y. (2011). Impacts of nanowhisker on formation kinetics and properties of all-cellulose composite gels. *Carbohydrate Polymers*, *83*(4), 1937–1946.

Yang, J., Han, C. R., Duan, J. F., Ma, M. G., Zhang, X. M., Xu, F., et al. (2012). Studies on the properties and formation mechanism of flexible nanocomposite hydrogels from cellulose nanocrystals and poly(acrylic acid). *Journal of Materials Chemistry*, *22*(42), 22467–22480.

Yang, J., Han, C. R., Duan, J. F., Xu, F., & Sun, R. C. (2013). Mechanical and viscoelastic properties of cellulose nanocrystals reinforced poly(ethylene glycol) nanocomposite hydrogels. *ACS Applied Materials & Interfaces*, *5*(8), 3199–3207.

Yang, X., Liu, Q., Chen, X., Yu, F., & Zhu, Z. (2008). Investigation of PVA/ws-chitosan hydrogels prepared by combined γ-irradiation and freeze–thawing. *Carbohydrate Polymers*, *73*(3), 401–408.

Zhang, L., Zhao, J., Zhu, J. T., He, C. C., & Wang, H. L. (2012). Anisotropic tough poly(vinyl alcohol) hydrogels. *Soft Matter*, *8*(40), 10439–10447.

Zhang, W., Yang, X. L., Li, C. Y., Liang, M., Lu, C. H., & Deng, Y. L. (2011). Mechanochemical activation of cellulose and its thermoplastic polyvinyl alcohol ecocomposites with enhanced physicochemical properties. *Carbohydrate Polymers*, *83*(1), 257–263.